PNAS RESEARCH ARTICLE | NEUROSCIENCE

Molecular signatures define subtypes of auditory afferents with distinct peripheral projection patterns and physiological properties

Caroline Siebald[a,1], Philippe F. Y. Vincent[b,1], Riley T. Bottom[a,1], Shuohao Sun[c,d,1], Daniel O. J. Reijntjes[b], Marco Manca[b], Elisabeth Glowatzki[a,b], and Ulrich Müller[a,2]

Edited by Robert Fettiplace, University of Wisconsin-Madison, Madison, WI; received October 5, 2022; accepted June 6, 2023

Type I spiral ganglion neurons (SGNs) are the auditory afferents that transmit sound information from cochlear inner hair cells (IHCs) to the brainstem. These afferents consist of physiological subtypes that differ in their spontaneous firing rate (SR), activation threshold, and dynamic range and have been described as low, medium, and high SR fibers. Lately, single-cell RNA sequencing experiments have revealed three molecularly defined type I SGN subtypes. The extent to which physiological type I SGN subtypes correspond to molecularly defined subtypes is unclear. To address this question, we have generated mouse lines expressing CreERT2 in SGN subtypes that allow for a physiological assessment of molecular subtypes. We show that *Lypd1-CreERT2* expressing SGNs represent a well-defined group of neurons that preferentially innervate the IHC modiolar side and exhibit a narrow range of low SRs. In contrast, *Calb2-CreERT2* expressing SGNs preferentially innervate the IHC pillar side and exhibit a wider range of SRs, thus suggesting that a strict stratification of all SGNs into three molecular subclasses is not obvious, at least not with the *CreERT2* tools used here. Genetically marked neuronal subtypes refine their innervation specificity onto IHCs postnatally during the time when activity is required to refine their molecular phenotype. Type I SGNs thus consist of genetically defined subtypes with distinct physiological properties and innervation patterns. The molecular subtype-specific lines characterized here will provide important tools for investigating the role of the physiologically distinct type I SGNs in encoding sound signals.

hearing | spiral ganglion neuron | hair cell | CreERT2 | inner ear

Significance

Afferent neurons within single sense organs have diverse properties that are crucial for information coding. Type I spiral ganglion neurons (SGNs) are the auditory afferents that transmit sound information to the brain. Several type I SGN subtypes have been distinguished by anatomical, electrophysiological, and molecular properties, but whether these properties are linked is unclear. By creating reporter lines for molecular type I SGN subtypes and characterizing their properties, we show that molecularly and physiologically defined SGN subtypes correlate only in part. Molecular subtypes consolidate their gene expression program and innervation specificity postnatally. The molecular subtype-specific lines characterized here are important tools for investigating the roles of physiologically distinct type I SGNs in sound coding.

The perception of sensory stimuli, such as light, smell, taste, touch, and sound, depends on specialized sensory neurons that transmit stimulus-evoked electrical signals to the central nervous system. These sensory afferents show variability in their properties even within a single sense organ. For example, in the mammalian retina, at least 30 different types of retinal ganglion cells have been observed (1, 2), suggesting that these afferent neurons contribute to the encoding of distinct visual features. In the mammalian inner ear, spiral ganglion neurons (SGNs) with different response properties and innervation patterns are thought to be important for the encoding of sound features such as intensity and pitch, as well as for pain and damage signaling (3–5). However, the extent to which afferent neurons within the inner ear are specialized to encode distinct features of auditory signals needs to be studied further.

Hair cells in the cochlear sensory epithelium of the inner ear are the primary sensory cells for the perception of sound. Two types of hair cells can be distinguished that are named inner hair cells (IHCs) and outer hair cells (OHCs) (Fig. 1*A*). OHCs are innervated by type II SGNs and have important functions in the amplification of sound signals. IHCs are innervated by type I SGNs that transmit sound information to the CNS and make up >95% of all SGNs. Each IHC is innervated monosynaptically by 5 to 30 type I SGNs that show striking variability in threshold, dynamic range, and spontaneous firing rates (SRs) (3, 5, 6). In several species, the distribution of type I SGNs with different SRs appears to be somewhat bimodal with a peak at low rates (≤1 spike/s) and higher rates (60 to 70 spikes/s) (7–12). Based originally on studies in cats, a subdivision of SGNs into three classes has been proposed: high-SR (>18 spikes/s), medium-SR (0.5 to 18 spikes/s), and low-SR (<0.5 spikes/s) fibers. This classification takes into account SRs and relative thresholds for activation by sensory input to encode sound over a wide intensity range (9). In cats, low- and high-SR fibers preferentially contact the modiolar and pillar sides of IHCs, respectively (Fig. 1*B*) (13). Morphological analysis in cats has also revealed that the largest synaptic ribbons face the modiolar side of IHCs (14), and intracellular labeling has demonstrated that

The authors declare no competing interest.

This article is a PNAS Direct Submission.

[1]C.S., P.F.Y.V., R.T.B., and S.S. contributed equally to this work.

[2]To whom correspondence may be addressed. Email: umuelle3@jhmi.edu.

This article contains supporting information online at https://www.pnas.org/lookup/suppl/doi:10.1073/pnas.2217033120/-/DCSupplemental.

Published July 24, 2023.

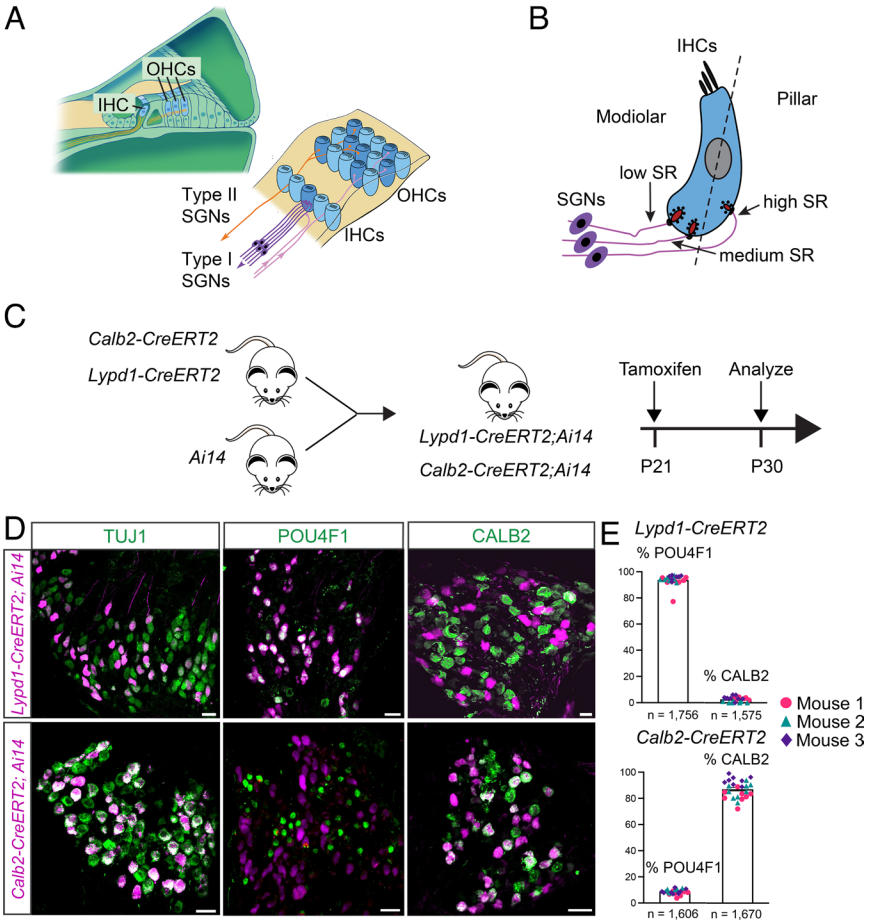

Fig. 1. Generation and characterization of *CreERT2* mice. (*A*) Diagram on the *Left*: cross-section of the cochlea: IHCs and OHCs. Diagram on the *Right*: *Top* view onto the cochlear epithelium showing IHCs, OHCs, SGNs type I (purple), SGNs type II (orange), and olivocochlear efferents (pink). (*B*) Diagram showing innervation of IHCs by SGNs with different spontaneous rates (SRs) along the modiolar to pillar axis. (*C*) Experimental strategy to label type IA and type IC SGNs using CreERT2 knock-in mouse lines. (*D*) Sections through the spiral ganglion of *Lypd1-CreERT2;Ai14* mice and *Calb2-CreERT2;Ai14* mice showing tdTomato expression (magenta) and stained with antibodies against TUJ1, POU4F1, or CALB2 (green). (*E*) Quantification of data in (*D*), % of tdTomato$^+$ SGNs in *Lypd1-CreERT2* (*Top*) and *Calb2-CreERT2* (*Bottom*) mice that express POU4F1 or CALB2 (n = number of neurons assessed). (Scale bars: 20 μm.)

these large ribbons oppose low-SR fibers (15). Similar observations have been made in guinea pigs (16). Studies in mice and rats support the view that single IHCs in rodents are innervated by fibers with different SRs (17–19). Furthermore, synapses on the pillar versus modiolar side of rodent IHCs differ in the sizes of presynaptic ribbons, postsynaptic AMPA receptor fields, and in their synaptic response properties to hair cell depolarization, specifically the IHC calcium channel properties that set the basic release rates (15, 17, 20–27). However, it has remained unclear whether rodent SGNs can be classified according to the scheme suggested in cats or whether the neurons show a more gradual difference in SRs along a continuum (19, 28–31). Notably, recent single-cell RNA sequencing (scRNAseq) studies in mice have demonstrated that type I SGNs can be classified into three subtypes that have been named type IA, IB, and IC (32–34). Based on these studies, it has been suggested that the three molecular subtypes in mice might correspond to physiological subtypes, similar to the physiological subtypes described in cats, although this has not been demonstrated experimentally. Transcriptional differences between type IA, IB, and IC neurons are for most genes not all or nothing but defined by gradual changes in a large set of genes (32–34). Thus, subdivision of afferent neurons into type I SGN subtype depends on the definition of threshold values for gene expression but might not capture graded functional differences between these neurons. The scRNAseq studies in mice open the door for a molecular exploration of the properties and functions of type I SGN subtypes.

To further define the diversity and function of type I SGNs in rodents, we have taken advantage of our published scRNAseq data (34) to identify genes that are suitable for the expression of *CreERT2* in molecularly defined type I SGN subtypes. This has allowed us to genetically mark subgroups of SGNs with fluorescent reporters. Here, we show that molecularly defined type I SGN subtypes have distinct developmental trajectories and innervation patterns onto IHCs and distinct SRs. By recording from the bouton endings of SGN dendrites to preserve spatial innervation information, we demonstrate that one group of type I SGNs that expresses *Lypd1-CreERT2* preferentially innervates the modiolar side of IHCs and has low SRs. A distinct group of SGNs that is labeled by the expression of *Calb2-CreERT2* preferentially innervates the pillar side of IHCs and shows a range of higher SRs. We also show that *Lypd1-CreERT2* and *Calb2-CreERT2* expressing neurons refine their innervation pattern onto IHCs in the postnatal phase coincident with the time frame when synaptic connections mature.

Overall, we conclude that molecularly defined type I SGN subclasses broadly correspond to anatomically and electrophysiological defined subclasses. However, unlike expectations, only the *Lypd1-CreERT2*-labeled neurons are a physiologically clearly defined group, while *Calb2-CreERT2*-labeled neurons have diverse physiological properties. The distinct gene expression patterns of these type I SGN subtypes might provide clues to the mechanisms that define differences in their innervation specificity and functional properties. The fact that the molecular and synaptic maturation of type I SGNs progresses during the time window when spontaneous and sensory-driven activity patterns are observed in the auditory system also suggests that activity-dependent mechanisms are perhaps of pivotal importance for regulating transcriptional programs and synaptic connectivity patterns in the auditory periphery.

Results

Characterization of *Calb2-CreERT2* and *Lypd1-CreERT2* Mice. In order to analyze the projection patterns, electrophysiological properties, and functions of type I SGN subtypes, we aimed to obtain mouse lines suitable for the genetic manipulation of these neurons. We examined scRNAseq data for genes that are differentially expressed between type IA, IB, and IC SGNs. Type I SGN subtypes can be distinguished by expression levels of specific marker genes, but expression differences are in most instances not all or nothing. One exception is the *Lypd1* gene, which is expressed at high levels in mature type IC SGNs only (32–35). A second gene that we explored is the *Calb2* gene, which is expressed at high levels in type IA SGNs, less in type IB SGN, and little if at all in type IC SGNs (32–35). We did not identify a gene that is only expressed in mature type IB SGNs without significant expression in other SGN subtypes. We therefore focused our studies on *Lypd1* and *Calb2*.

To characterize type IA SGNs, we obtained *Calb2-CreERT2* mice that have been described previously (36). These mice contain a knock-in of *CreERT2* into the genomic locus of the *Calb2* gene simultaneously leading to the inactivation of *Calb2*. For type IC SGNs, we used CRISPR gene targeting to insert *CreERT2* just before the stop codon of the last *Lypd1* coding exon. The *Lypd1* and *CreERT2* coding regions were separated by a viral 2A-like peptide (T2A), which, during translation, forces the ribosome to skip without forming a peptide bond (37). Thus, an independent CreERT2 protein is generated while also maintaining LYPD1 expression.

To characterize *Calb2-CreERT2* and *Lypd1-CreERT2* mice, we crossed them to *Ai9* and *Ai14* mice, which contain a Cre-inducible *tdTomato* transgene (Fig. 1*C*) (38). Both fluorescence reporter lines gave similar results and were used interchangeably. To analyze CreERT2-mediated recombination patterns in differentiated neurons, we intraperitoneally injected mice heterozygous for the *CreERT2* transgene and for tdTomato at P21 with tamoxifen (0.1 mg/g body weight) and analyzed sections of the spiral ganglion at P30 for tdTomato expression. Sections were also stained for known molecular markers for type I SGNs using immunohistochemistry. As molecular markers, we used TUJ1, which is expressed in all adult type I SGNs (39, 40), as well as CALB2 and POU4F1, which are prominently expressed in type IA and type IC SGNs, respectively (34). In *Calb2-CreERT2;Ai9/14* mice, tdTomato was expressed in $TUJ1^+$ type I SGNs that also expressed CALB2 but little if any POU4F1 (Fig. 1 *D* and *E*). In *Lypd1-CreERT2;Ai9/14* mice, tdTomato was expressed in $TUJ1^+$ type I SGNs that also expressed POU4F1, but minimally expressed CALB2 (Fig. 1 *D* and *E*). We conclude that at P21, the *Calb2-CreERT2* and *Lypd1-CreERT2* mouse lines largely exhibit nonoverlapping expression patterns in distinct subtypes of mature type I SGNs.

To exclude that the tamoxifen dose that we used only led to partial activation of Cre recombination, we injected mice intraperitoneally between P21 and P28 with several doses of tamoxifen or its more potent metabolite 4-hydroxy-tamoxifen. Following 4-hydroxy-tamoxifen injection at P21/P22 in *Calb2-CreERT2*; *Ai14* mice, we obtained similar results as with a single injection of tamoxifen at P21 (P21 tamoxifen: 50.89% SGNs; P21/22 4-hydroxy-tamoxifen: 50.78% SGNs). We also attempted to characterize Cre expression by immunohistochemistry with several Cre antibodies, but in each instance, nonspecific background staining was too prevalent to draw firm conclusion. Overall, our findings suggest that one dose of tamoxifen injection fully captured all type I SGNs that express CreERT2 at sufficiently high levels to induce Cre recombination. Calb2-CreERT2 might be expressed at lower levels in additional neurons, but expression levels are likely below the levels that are necessary to induce recombination of target genomic loci.

Developmental Refinement of *Calb2-CreERT2* and *Lypd1-CreERT2* Expression. It has previously been shown that the expression of *Calb2* and *Lypd1* is refined between P0 and P28 to subgroups of neurons within the entire SGN population. *Calb2* is initially broadly expressed at lower levels in most SGNs but is at P21 expressed at high levels in type IA neurons, at intermediate levels in type IB neurons, and not at all or at very low levels in type IC neurons (32–34). *Lypd1* is by P0 already confined to approximately 70% of all type I SGNs and by P21 is restricted to the ~34% of type IC SGNs (32–34). To further characterize our *CreERT2* mice, we analyzed the extent to which they recapitulated this developmental change in the expression patterns of the endogenous genes.

First, we injected different cohorts of *Calb2-CreERT2;Ai9* mice at P1 or P21 with tamoxifen (0.1 mg/g body weight). We then analyzed in both cohorts sections of the spiral ganglion at P28 for tdTomato expression (Fig. 2 *A* and *B*). We used TUJ1 as a generic marker for all type I SGNs (39, 40). In *Calb2-CreERT2;Ai9* mice injected at P1 with tamoxifen, 55% of $TUJ1^+$ neurons expressed tdTomato at P28, while in those injected with tamoxifen at P21, 51% of $TUJ1^+$ neurons expressed tdTomato at P28. The vast majority (≥97%) of *Calb2-CreERT2*-labeled SGNs did not express the SGN type IC marker POU4F1 regardless of the time point of tamoxifen injection, indicating that transgene expression was excluded from type IC SGNs (Fig. 2 *C* and *D*). Twenty-seven percent of the neurons labeled in *Calb2-CreERT2;Ai9* mice by injection of tamoxifen at P1 expressed at P28 the SGN type IB marker CALB1. This number was reduced to 15% when tamoxifen was injected at P21 (Fig. 2 *E* and *F*). These findings are consistent with recent scRNAseq studies that have shown that the segregation of type I SGNs into molecular subclasses is already observed at birth with a further refinement of gene expression at subsequent ages (32, 33, 35, 41). To rule out incomplete tamoxifen-mediated activation, we also treated *Calb2-CreERT2; Ai14* mice with 2 doses of 4-hydroxy-tamoxifen at P1/2 and found a minor increase in $tdTomato^+$ SGNs at P28 (62% of the total $TUJ1^+$ population) versus single injection of tamoxifen at P1 (55%). Thus, while low levels of CALB2 expression are observed in nearly all type I SGNs at birth (34), *Calb2-CreERT2* was likely expressed at sufficiently high levels only in the type IA SGNs with the highest CALB2 expression levels, as well as some expression in type IB neurons that express lower levels of CALB2. In contrast, *Calb2-CreERT2* expression was excluded from type IC SGNs.

Following tamoxifen injection into *Lypd1-CreERT2;Ai14* mice at P1, tdTomato expression at P28 was confined to 60% of $TUJ1^+$ type I SGNs (Fig. 3 *A* and *B*). These neurons did not express significant levels of CALB2 (Fig. 3 *C* and *D*), suggesting that they were distinct from type IA neurons. However, the neurons expressed CALB1 (Fig. 3 *E* and *F*), suggesting that they represented both type IB and IC neurons (Fig. 3*C*). Type I SGNs in *Lypd1-CreERT2* mice labeled by tamoxifen injection at P21 became restricted to 28% of the total pool of type I SGNs and did not express CALB1 or CALB2, confirming a postnatal refinement of Lypd1 expression leading to its maintenance in type IC SGNs only.

Analysis of SGN Projection Patterns Using *Calb2-CreERT2* and *Lypd1-CreERT2* Mice. Previous studies suggest that type IA SGNs might preferentially target the pillar side of IHCs, while type IC SGNs might preferentially target the modiolar side, with type IB

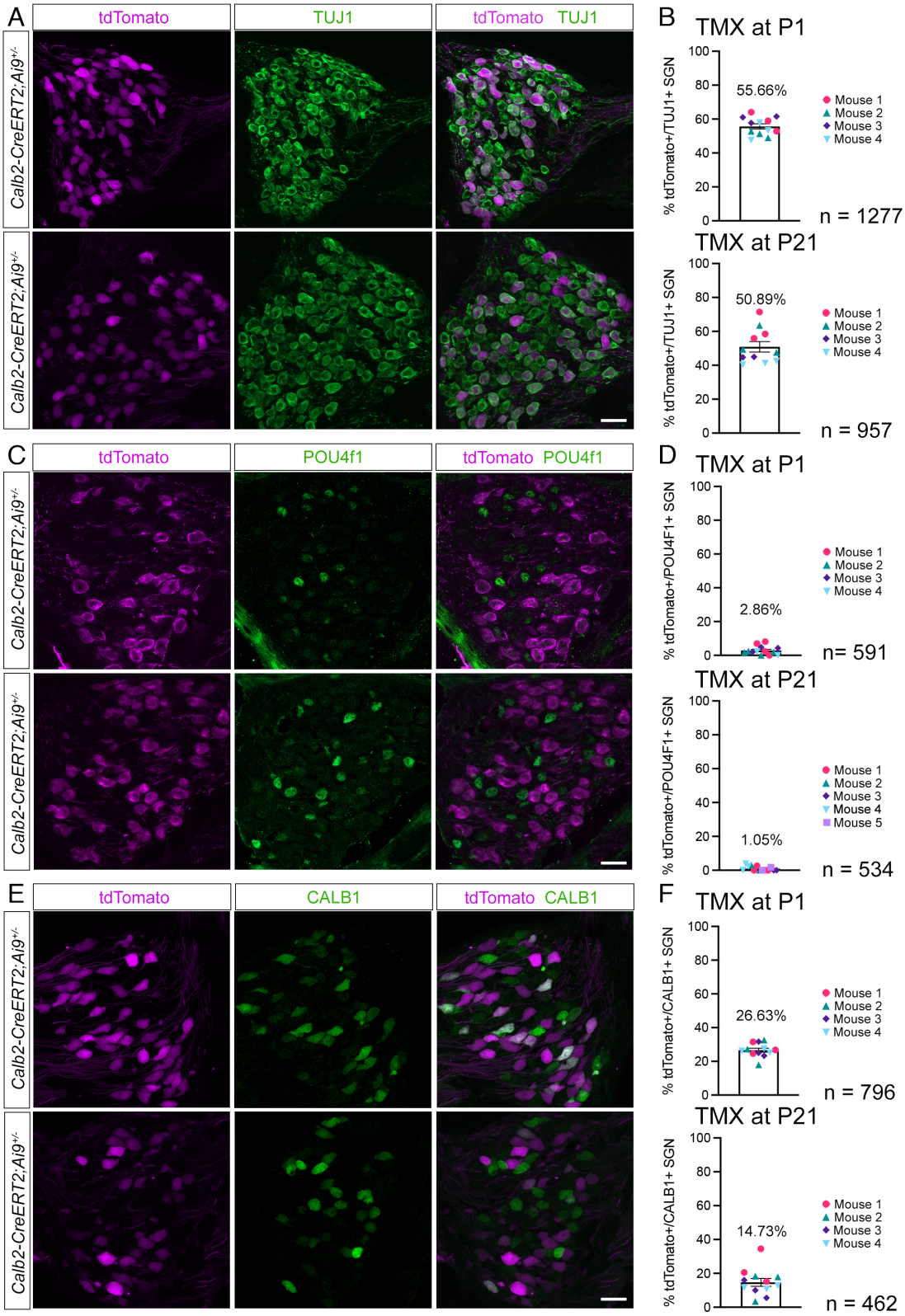

Fig. 2. Developmental refinement of *Calb2-CreERT2* expression. Sections through the spiral ganglions of P28 *Calb2-CreERT2;Ai9* animals injected with tamoxifen (TMX) at either P1 or P21, stained with the indicated antibodies. *Upper* panels show sections from animals injected with TMX at P1, and *Lower* panels show sections from animals injected with TMX at P21. (*A*) Sections stained with antibodies against tdTomato (magenta) and TUJ1 (green). (*B*) Percentage of TUJ1$^+$ cells colabeled with tdTomato after TMX injection at P1 versus P21. (*C*) Sections stained with antibodies against tdTomato (magenta) and POUF4F1 (green). (*D*) Percentage of tdTomato$^+$ cells colabeled with POU4F1 after TMX injection at P1 versus P21. (*E*) Sections stained with antibodies against tdTomato (magenta) and CALB1 (green). (*F*) Percentage of tdTomato$^+$ cells colabeled with CALB1 after TMX injection at P1 versus P21. (n = number of neurons assessed). (Scale bars: 20 μm.)

fibers terminating more medially (Fig. 1*B*) (32–34). To test this model, we analyzed the projection patterns of SGN fibers that were labeled in our *CreERT2* mice by the expression of fluorescence marker genes. We used different strategies to characterize SGN projection patterns in *Calb2-CreERT2* and *Lypd1-CreERT2* mice. For projection tracing in *Calb2-CreERT2* animals, we had to

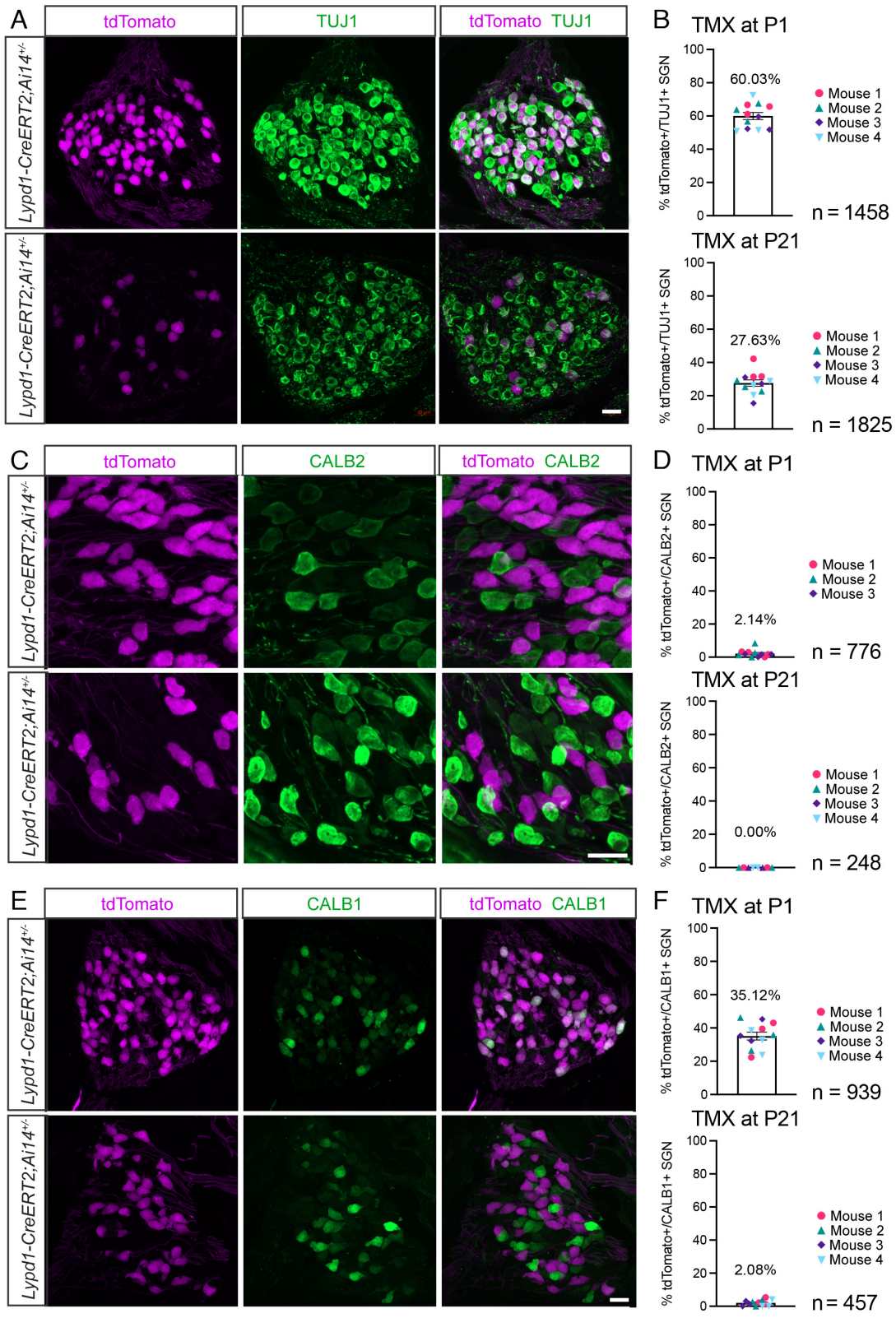

Fig. 3. Developmental refinement of *Lypd1-CreERT2* expression. Sections through the spiral ganglions of P28 *Lypd1-CreERT2;Ai14* animals injected with tamoxifen (TMX) at either P1 or P21, stained with the indicated antibodies. *Upper* panels show sections from animals injected with TMX at P1, and *Lower* panels show sections from animals injected with TMX at P21. (*A*) Sections stained with antibodies against tdTomato (magenta) and TUJ1 (green). (*B*) Percentage of TUJ1$^+$ cells colabeled with tdTomato after TMX injection at P1 versus P21. (*C*) Sections stained with antibodies against tdTomato (magenta) and CALB2 (green). (*D*) Percentage of tdTomato+ cells colabeled with CALB2 after TMX injection at P1 versus P21. (*E*) Sections stained with antibodies against tdTomato (magenta) and CALB1 (green) after TMX injection at P1 or P21. (*F*) Percentage of tdTomato$^+$ cells colabeled with CALB1 after TMX injection at P1 versus P21 (n = number of neurons assessed). (Scale bars: 20 μm.)

take into consideration that IHCs express CALB2 (42), which would mask the fluorescence signal from the thin dendrites of SGNs innervating IHCs. We therefore took advantage of an AAV vector containing a Cre-inducible fluorescence reporter that is expressed from the neuron-specific synapsin promoter (AAV9-hSyn-DIO-EGFP). Following injection of this AAV vector into

Calb2-CreERT2 mice and tamoxifen administration, expression of the EGFP fluorescence marker is expected to be confined to SGNs. We injected AAV9-hSyn-DIO-EGFP into the semicircular canal of *Calb2-CreERT2* mice at P2 followed by intraperitoneal injection of a low dose of tamoxifen (50 μg/animal) at P21 and tissue harvest at P28 (Fig. 4*A*). For projection tracing in *Lypd1-CreERT2* mice, we crossed these mice to *Ai14* reporter mice and injected the offspring at P21 intraperitoneally with tamoxifen (50 μg/animal) followed by tissue harvest at P28 (Fig. 4*E*).

Using confocal fluorescence microscopy, we imaged cochlear whole mounts and analyzed optical sections for the expression of fluorescence markers. Hair cells were visualized by staining with antibodies to CALB1 or MYO7A (Fig. 4 *C* and *F*). To quantify the position at which peripheral SGN projections innervated IHCs, we determined for each innervating fiber the "Normalized Basal Position" (NBP) as described (18) (Fig. 4*B*). For this purpose, we analyzed consecutive optical sections through the cell body of hair cells to draw an imaginary axis aligned through the cuticular plate and nucleus to divide IHCs into pillar and modiolar sides (Fig. 4*B*, dotted lines). The position of innervation was then determined relative to this imaginary axis. NBP is positive for modiolar-side terminals and negative for pillar-side terminals (set by S which is ±1; the 0 position defines fibers innervating hair cells medially). In *Calb2-CreERT2* mice, the vast majority of EGFP-labeled neurons innervated the basal aspect of IHCs toward the pillar side (Fig. 4 *C* and *D*), while in *Lypd1-CreERT2* mice, the vast majority of tdTomato-labeled neurons innervated the basal aspect of IHCs toward the modiolar side (Fig. 4 *F* and *G*). In *Calb2-CreERT2* mice, significant numbers of labeled nerve fibers also contacted the middle and modiolar side of hair cells (Fig. 4*D*, which is likely explained by the expression of the *CreERT2* transgene in type IB neurons (Fig. 2).

Postnatal Refinement of the Innervation Specificity of *Lypd1-CreERT2* and *Calb2-CreERT2*-Labeled Neurons. The mechanisms that determine how type I SGNs establish their innervation specificity along the modiolar to pillar axis of IHCs are not known. To address this issue, we carried out additional experiments. We focused on the postnatal refinement process in *Lypd1-CreERT2* and *Calb2-CreERT2* mice because at prenatal ages, expression of *Lypd1* and *Calb2* is not yet refined to type I A and type I B/C SGNs, respectively (35, 43). To sparsely label neurons, we injected

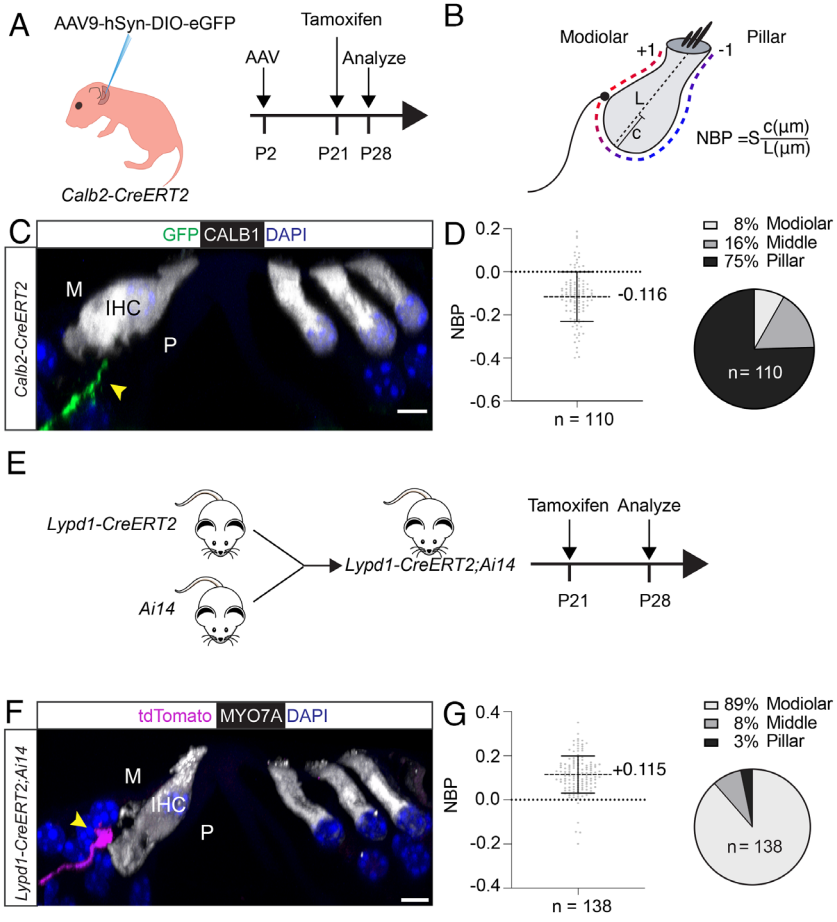

Fig. 4. Peripheral projection patterns of type I SGNs labeled by *Calb2-CreERT2* and *Lypd1-CreERT2* expression. (*A*) Diagram of experimental strategy to label nerve fibers in *Calb2-CreERT2* animals. (*B*) Diagram of SGN type I innervation location assessment at the IHC using the method by Markowitz and Kalluri (18), NBP: normalized basal position; L: length of hair cell; c: distance between fiber ending position and basal pole of hair cell; S: set at +1 or −1 to define modiolar versus pillar, with a value of 0 for medial basal pole. (*C*) Representative example of P28 midcochlear section in a *Calb2-CreERT2* animal; hair cells stained with CALB1 (white); a GFP-labeled fiber (green, arrow) innervates an IHC on the pillar side (P), nuclei are stained with DAPI (blue). (*D*) Quantification of innervation in P28 *Calb2-CreERT2* animals; *Left*: NBP assessed across 110 virally labeled neurons from 3 animals; *Right*: modiolar versus pillar innervation assessed for 110 neurons from 3 animals. The fractional distance of the contact position from the basal pole of the hair cell was determined by dividing c by L and multiplying the resulting number by S (+1 or −1, for innervations on the modiolar or pillar sides of the bisecting plane, respectively; values for middle were at 0). (*E*) Diagram of experimental strategy to label nerve fibers in *Lypd1-CreERT2;Ai14* animals. (*F*) Representative example of P28 midcochlear section in *Lypd1-CreERT2;Ai14* animal; hair cells stained with MYO7A (white); a tdTomato-labeled fiber (magenta, arrow) innervates an IHC on the modiolar side (M), nuclei are stained with DAPI (blue). (*G*) Quantification of innervation in P28 *Lypd1-CreERT2;Ai14* animals; *Left*: NBP assessed across 138 labeled fibers from 3 animals; *Right*: modiolar versus pillar innervation assessed across 138 labeled fibers from 3 animals. (Scale bar: 5 μm.)

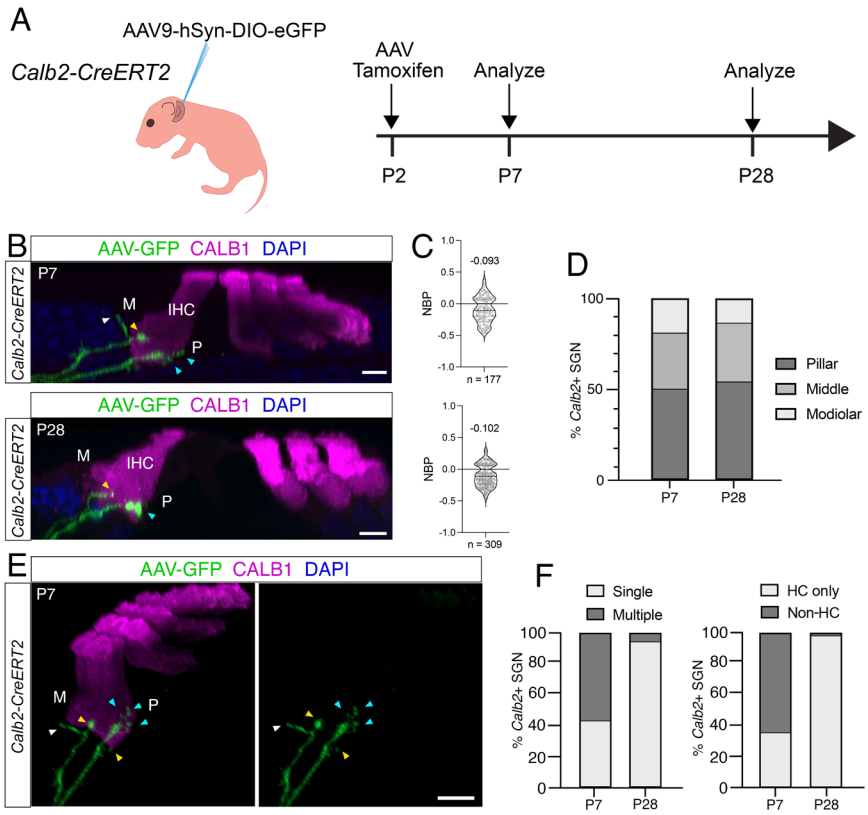

Fig. 5. Developmental analysis of peripheral projection patterns of type I SGNs labeled by *Calb2-CreERT2* expression at P2. (*A*) Experimental strategy for assessment of projection refinement in *Calb2-CreERT2* animals; *Left*: diagram of injection of AAV9-hSyn-DIO-eGFP into the posterior semicircular canal of *Calb2-CreERT2* animals at P2; *Right*: experimental timeline. (*B*) Mid-cochlear sections of cochleae from *Calb2-CreERT2* animals collected at P7 (*Top*) or P28 (*Bottom*); hair cells (magenta) including IHC labeled with indicated antibodies; modiolar (M) and pillar (P) sides of IHC highlighted; virally labeled fibers (green) indicated by arrows. (*C*) Quantification of innervation positions for virally labeled fibers from samples collected at P7 (*Top*) and P28 (*Bottom*) using NBP [see legend to Fig. 4; Markowitz and Kalluri (18)]. A total of 177 fibers and 309 fibers from three animals were evaluated at P7 and P28, respectively. (*D*) Quantification of modiolar versus pillar innervation for virally labeled fibers from samples collected at P7 (*Left*) and P28 (*Right*). (*E*) Innervation details for virally labeled fibers at P7 indicating excess contacts with IHC (yellow arrows), forming several branches on the modiolar (M) side of a single IHC (blue arrows) and projections away from IHC (white arrow). (*F*) Quantification of terminal peripheral projections by *Calb2-CreERT2*-labeled neurons at P7 versus P28; *Left*: % of *Calb2-CreERT2*$^+$ neurons exhibiting single versus multiple terminal branches to IHCs at P7 (*Left*) or P28 (*Right*); *Right*: % of *Calb2-CreERT2*$^+$ neurons with only branches terminating at IHCs (HC only) versus neurons that feature branches extending away from the IHC (Non-HC). (Scale bars: 5 μm.)

Lypd1-CreERT2 and *Calb2-CreERT2* mice with Cre-dependent AAV9-hSyn-DIO-EGFP (Figs. 5*A* and 6*A*). The combination of virus infection with tamoxifen induction allowed for very sparse labeling of axonal projections, thus facilitating fine-mapping of nerve endings. AAV injections and tamoxifen treatment were carried out at P2, and projection patterns of labeled neurons were visualized at P7 and P28. At P7, the labeled SGN fibers in *Calb2-CreERT2* mice showed a clear preference for the pillar side of IHCs but also extend more medially and even to the modiolar side of IHCs (Fig. 5 *B*–*D*). A similar innervation specificity was

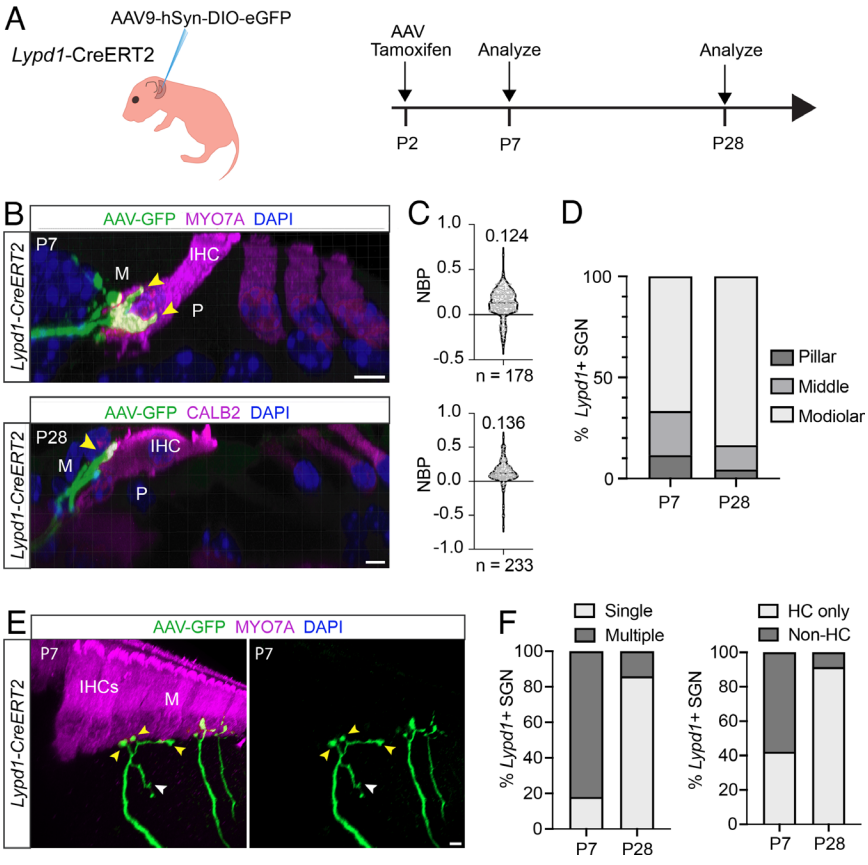

Fig. 6. Developmental analysis of peripheral projection patterns of type I SGNs labeled by *Lypd1-CreERT2* expression at P2. (*A*) Experimental strategy for assessment of projection refinement in *Lypd1-CreERT2* animals; *Left*: diagram of injection of AAV9-hSyn-DIO-eGFP into the posterior semicircular canal of *Lypd1-CreERT2* animals at P2; *Right*: experimental timeline. (*B*) Midcochlear sections of cochleae from *Lypd1-CreERT2* animals collected at P7 (*Top*) or P28 (*Bottom*); hair cells (magenta) including IHC labeled with indicated antibodies; modiolar (M) and pillar (P) sides of IHC highlighted; virally labeled fibers (green) indicated by arrows. (*C*) Quantification of innervation positions for virally labeled fibers from samples collected at P7 (*Top*) and P28 (*Bottom*) using NBP [see legend to Fig. 4; Markowitz and Kalluri (18)]. A total of 178 fibers and 233 fibers from three animals were evaluated at P7 and P28, respectively. (*D*) Quantification of modiolar versus pillar innervation for virally labeled fibers from samples collected at P7 (*Left*) and P28 (*Right*). (*E*) Innervation details for virally labeled fibers at P7 indicating excess contacts with IHC (yellow arrows) and projections away from IHC (white arrow) on the modiolar (M) side. (*F*) Quantification of terminal peripheral projections by *Lypd1-CreERT2*-labeled neurons at P7 versus P28; *Left*: % of *Lypd1-CreERT2*$^+$ neurons exhibiting single versus multiple terminal branches to IHCs at P7 (*Left*) or P28 (*Right*); *Right*: % of *Lypd1-CreERT2*$^+$ neurons with only branches terminating at IHCs (HC only) versus neurons that feature branches extending away from the IHC (Non-HC). (Scale bars: 5 μm.)

observed at P28. Nerve fibers at P7 frequently formed several branches onto hair cells or even projected away from hair cells, but these excess projections were no longer detectable at P28 (Fig. 5 *E* and *F*). Similar observations were made in *Lypd1-CreERT2* mice, although in this case, the labeled nerve fibers at P7 showed already a clear preference for the modiolar side of hair cells and projections to the pillar side were very rare (Fig. 6 *B*–*D*). Similar to *Calb2-CreERT2*-labeled fibers, *Lypd1-CreERT2*-labeled fibers underwent a refinement process. Nerve fibers frequently formed branches near their final tips and contacted more than one IHC toward the modiolar side (Fig. 6 *E* and *F*). In contrast, SGNs for animals killed at P28 very rarely exhibited any branching (Fig. 6*F*).

Spontaneous Firing Rates of SGN Subtypes. Based on studies in cats, SGNs have been grouped into low, medium, and high SR fibers based on the profile and local maxima of the SR distribution (9). Recordings in several other species including rodents suggest that type I SGNs also have a similarly wide range of SRs, but they cannot easily be classified into groups due to lack of local maxima in the distribution (19, 28–31). To analyze type I SGNs further, we recorded SRs of nerve fibers innervating IHCs along the modiolar to pillar axis in *Calb2-CreERT2* and *Lypd1-CreERT2* mice. Since CALB2 is also expressed in IHCs, type IA/B fibers in *Calb2-CreERT2* mice were labeled by injection of AAV9-hSyn-DIO-eGFP at P2, followed by tamoxifen (50 μg/animal) treatment at P21. To label type IC fibers in *Lypd1-CreERT2* mice, these mice were crossed with *Ai14* mice and treated with tamoxifen (50 μg/animal) at P21. Recordings were performed in apical turns of 3 to 4-wk-old acutely excised tissue focusing on mice with sparsely labeled nerve projections that allowed us to observe individual nerve endings.

Extracellular loose-patch recordings reporting spike timing were performed from SGN bouton endings close to where they contact IHCs (Fig. 6 *A*–*C*) (19). Recordings were performed at room temperature with extracellular 1.3 mM Ca^{2+} and 5.8 mM K^+, conditions defined as resulting in a range of SRs in vitro with "low" to "high" SR fibers. This SR distribution, when scaled to body temperature conditions, reflects the SR range found in vivo (19). By focusing through differential interference contrast (DIC) images, IHCs were divided into pillar and modiolar sides by an imaginary axis aligned through the cuticular plate and nucleus (Fig. 6 *A* and *B*, dotted lines). SRs were monitored for 3 min, and SR was determined over the last 2 min and linked to the SGN ending position on the IHC. We recorded from unlabeled and labeled fibers to capture the full range of SRs of all fibers. Fluorescently labeled fibers were identified by the labeled boutons at the tip of the patch pipette and the labeled SGN membrane invaginating into the pipette (*Insets*, Fig. 7 *A* and *B*, arrowheads).

We first analyzed SRs of type I SGN fibers in *Calb2-CreERT2* mice (Fig. 7 *A*, *C*, *D*, and *F*). As expected, imaging of excised live tissue from 4-wk-old *Calb2-CreERT2* mice showed that nearly all GFP-labeled fibers contacted the basal aspect of IHCs toward the pillar side with very few fibers innervating the modiolar side (Fig. 7*A*, white arrows). When analyzing both unlabeled and labeled nerve fibers in *Calb2-CreERT2* mice, we observed a wide range of SRs that defied easy classification into distinct groups (Fig. 7 *D* and *F*). During recordings, CALB2-positive fibers could not be unambiguously identified as pillar or modiolar due to the more basal contact locations. However, for unlabeled fibers with identified pillar/modiolar contact location, there was a clear modiolar to pillar gradient in SRs (Fig. 7*D*). Unlabeled fibers that innervated the modiolar side (modiolar no-fluo) of IHCs had SRs ranging from 0.042 to 31.13 spikes/s, while fibers innervating the pillar side of IHCs (pillar no-fluo) had SRs ranging from 0.59 to 47.94 spikes/s. Mean values were 7.62 ± 9.45 spikes/s and 21.91 ± 16.36 spikes/s, respectively. SRs of modiolar fibers were thus significantly lower than those of pillar fibers (Fig. 7*D*) (P = 0.038, Kruskal–Wallis test). Next, we compared SRs of GFP-labeled nerve fibers to SRs in pillar or modiolar nerve fibers without fluorescence. Fibers labeled with GFP displayed a range of SRs from 0.48 to 19.74 spikes/s with a mean value of 8.59 ± 6.31 spikes/s (Fig. 7 *D* and *F*; green dots, n = 9). Mean SRs of GFP-labeled fibers in *Calb2-CreERT2* mice were not statistically different from either unlabeled modiolar "No Fluo" fibers (7.62 ± 9.45 spikes/s, n = 12, $P > 0.99$, Kruskal–Wallis test) and unlabeled pillar No Fluo fibers (21.91 ± 16.36 spikes/s, n = 12, P = 0.29, Kruskal–Wallis test).

We conclude that *Calb2-CreERT2* labels a population of type IA/IB SGNs with a broad range of SRs that tend to innervate the basal aspect of IHCs toward the pillar side. Notably, *Calb2-CreERT2* failed to label fibers with the highest SRs, indicating that *Calb2-CreERT2* may not label all type IA SGNs equally.

Next, we analyzed SRs of tdTomato$^+$ and tdTomato$^-$ SGN fibers in *Lypd1-CreERT2;Ai14* mice. As expected, imaging of the excised live tissue from 4-wk-old *Lypd1-CreERT2;Ai14* mice showed that nearly all tdTomato-labeled fibers contacted the basal aspect of IHCs toward the modiolar side (Fig. 7*B*). When considering all nerve fibers irrespective of tdTomato expression, we observed that type I SGNs had a large range of SRs (Fig. 7*G*). We noted a similar modiolar to pillar gradient in SRs as for *Calb2-CreERT2* mice, indicating that SR is not influenced by the *CreERT2* transgene in the two mouse lines under study (Fig. 7 *F* and *G*). Fibers labeled with tdTomato had low SRs with a mean value of 0.47 ± 0.73 spikes/s (Fig. 7*E*; magenta dots; n = 8) and had significantly slower SRs compared to the unlabeled No Fluo pillar fibers (21.49 ± 15.45 spikes/s, n = 12, $P < 0.001$, Kruskal–Wallis test) but were not significantly different from the unlabeled No Fluo modiolar fibers (6.91 ± 8.89 spikes/s, n = 10, P = 0.30, Kruskal–Wallis test). We conclude that *Lypd1-CreERT2* labels a population of type IC SGNs with low SRs that tend to innervate the basal pole of IHCs toward the modiolar side.

Discussion

The auditory system has an extraordinary signaling capability representing sounds over a wide range of frequencies and intensities by mechanisms that are not fully understood. Frequency discrimination is achieved at least in part by using the information provided by the tonotopic organization of the auditory system. Intensity coding depends on nonlinear amplification of sound signals by OHCs that is modulated by efferent feedback (44). Differences in the properties of auditory afferent neurons are also thought to play crucial roles in the encoding of sound features. However, the extent to which genetically hardwired and activity-dependent mechanisms contribute to the functional diversification of type I SGNs still needs to be explored. To begin addressing these questions, we have taken advantage of our previously described scRNAseq data to generate genetic tools that allow us to access molecular subclasses of type I SGNs to define their developmental trajectories, circuit diagrams, electrophysiological properties, and functions.

Using mouse lines expressing *CreERT2* from endogenous genetic loci, we provide here further evidence that type I SGNs are a diverse group of neurons and that their diversity can be captured at least in part by differences in their gene expression program. Our data also show that molecularly defined type I SGN subtype and physiological subtype correspond at first approximation to each other. Accordingly, mouse lines expressing *Calb2-CreERT2* and *Lypd1-CreERT2* are expressed in different sets of SGNs with minimal coexpression in a small subset of neurons. *Calb2-CreERT2* labels type IA/B SGNs with a wider range of SRs compared to *Lypd1-CreERT2*-labeled type IC SGNs with low SRs. *Calb2-CreERT2*-labeled neurons innervate

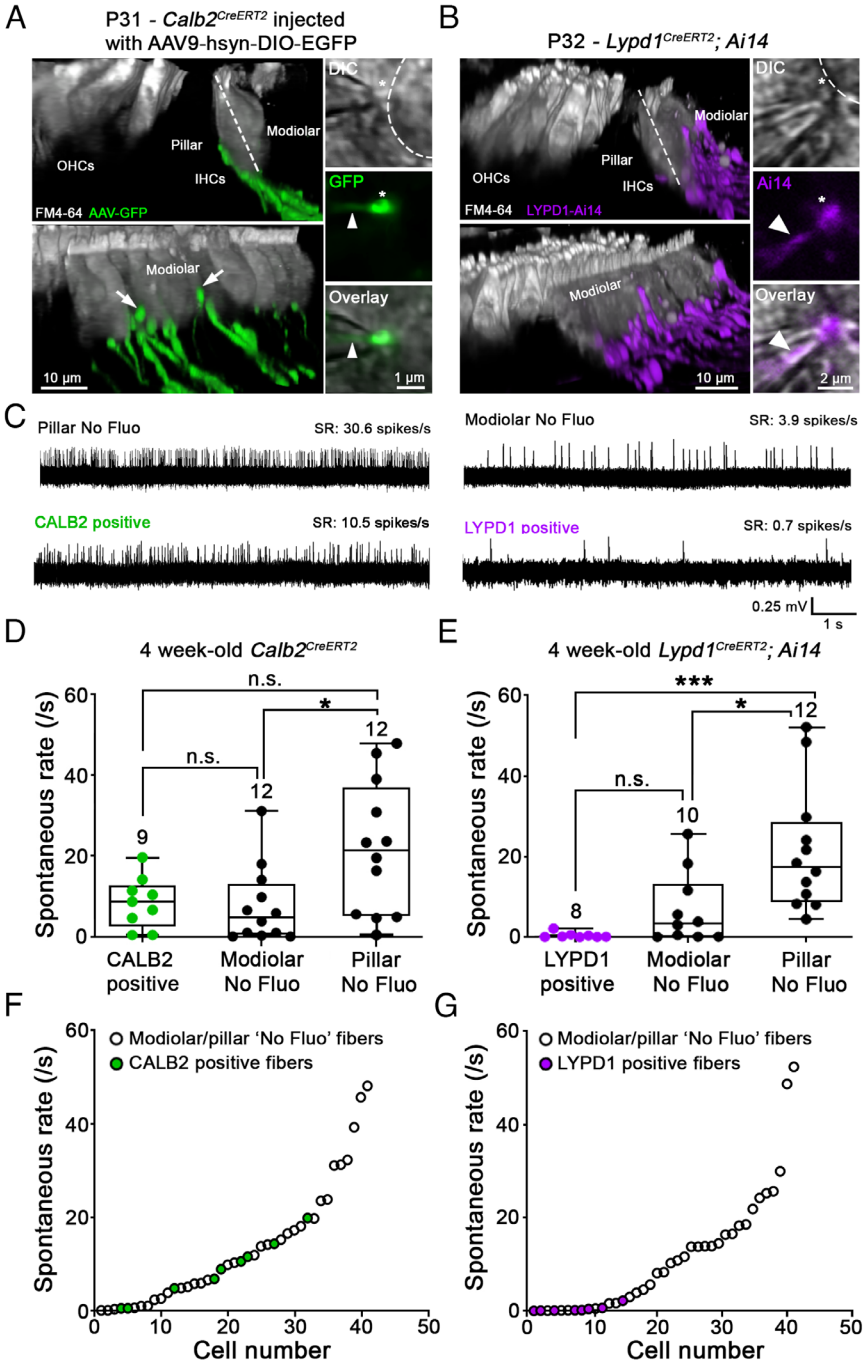

Fig. 7. Recording of spontaneous firing rates from SGN bouton endings in *CALB2-CreERT2* and *Lypd1-CreERT2* and mice. (*A* and *B*) Confocal z-stack reconstructions captured from live tissue of acutely excised apical turns of the organ of Corti at ~4 wk of age. *Left*, two side views at different angles showing OHCs and IHCs (gray). IHCs are contacted by fluorescing fibers, preferentially (*A*) on the pillar side in *Calb2-CreERT2* mice that were injected with AAV9-hSyn-DIO-EGFP at P2 (green) and (*B*) on the modiolar side in *Lypd1-CreERT2;Ai14* mice (magenta), followed by tamoxifen injection at P21. A few labeled nerve fibers in *Calb2-CreERT2* mice can be observed contacting IHCs on the modiolar side (white arrows). *Right,* two-dimensional confocal snapshots of DIC view (*Top*), 488 nm (green) or 568 nm (magenta) fluorescence (*Middle*), and DIC and fluorescence overlayed (*Bottom*). The overlay shows a fluorescent bouton ending (asterisk) slightly invaginated into a pipette tip (arrow head) for loose-patch recording, thereby confirming the recording of labeled fiber in *Calb2-CreERT2* (*A*) and *Lypd1-CreERT2;Ai14* (*B*) mice. (*C*) Four example traces of extracellular loose-patch recordings for individual SGN fibers showing different SRs (CALB2$^+$; LYPD1$^+$; pillar and modiolar fibers without fluorescence ("No Fluo"). (*D*) Comparison of spontaneous firing rate between fibers labeled in *Calb2-CreERT2* mice (green), modiolar No Fluo fibers (black) and pillar No Fluo fibers (black) obtained ~4-wk-old animals. Boxes represent the 10th to 90th percentile of the distribution and whiskers the minimum and maximum values. The horizontal line represents the median. (Kruskal–Wallis test with Dunn's multiple comparison; n.s. not significant, *P < 0.05 and ***P < 0.001). (*E*) Comparison of SRs between fibers labeled in *Lypd1-CreERT2;Ai14* mice (red), modiolar No Fluo fibers (black) and pillar No Fluo fibers (black) from ~4-wk-old animals. Same statistical tests as in (*D*). (*F* and *G*) Distribution of spontaneous firing rate from the lowest to the highest SR in *Calb2-CreERT2* (*F*) and *Lypd1-CreERT2;Ai14* (*G*) mouse lines; same data as in (*D* and *E*). Each dot corresponds to a single SGN bouton recording whereby green dots represent GFP$^+$ fibers in *Calb2-CreERT2* animals and red dots tdTomato$^+$ fibers in *Lypd1-CreERT2;Ai14* animals. Note that SRs of tdTomato$^+$ fibers in *Lypd1-CreERT2; Ai14* mice are observed at the lower end of the SR range, whereas SRs of GFP$^+$ fibers in *Calb2-CreERT2* mice occupy a wider middle range. ANF recordings were performed from 34 animals, 17 animals per mouse line. The number above each bar represents the number of recorded fibers.

IHCs preferentially but not exclusively on the pillar side, while almost all *Lypd1-CreERT2*-labeled neurons innervate IHCs on the modiolar side. This is consistent with previous studies in cats, which have shown that high SR fibers tend to innervate IHCs on the pillar side and low SR fibers on the modiolar side, respectively (13). Notably, *Calb2-CreERT2* does not label nerve fibers with the highest SRs. This could indicate additional genetic variability in the pool of type IA SGNs or reveal a limitation in our Cre tool that might only reveal a subset of type IA SGNs or does not label all fine processes well enough to visualize them in live tissue for recordings. Alternatively, it could indicate a bias in the selection of fibers captured for recordings.

Calb2-CreERT2 and *Lypd1-CreERT2* label already at P1 non-overlapping sets of neurons, which is consistent with recent data from scRNAseq studies that have provided evidence that type IA (high CALB2, low CALB1, and no LYPD1) and type IC (high LYPD1, low CALB2, and low CALB1) neurons belong to distinct developmental lineages that are established at birth (35, 43). In addition, both *Calb2-CreERT2* and *Lypd1-CreERT2* are expressed at birth in type IB SGNs (high CALB1, low CALB2, and no LYPD1), but their expression is subsequently refined. At P21, *Calb2-CreERT2* labels a smaller population of type IB SGNs compared to P1, while *Lypd1-CreERT2* no longer labels type IB SGNs by P21. The *CreERT2* mice thus recapitulate the postnatal refinement in the gene expression pattern of type I SGNs previously observed by scRNAseq studies and immunohistochemistry (33, 34). The findings also suggest that lineage relationships between type IB neurons with type IA and type IC neurons may not be

fully resolved at birth. Alternatively, it might be difficult to decipher the full complement of lineage relationships with our genetic marking studies that rely on single transgenes.

Our data provide insights into the timeline when type I SGN subtypes refine their innervation specificity onto IHCs. Previous studies had already provided evidence that type I SGNs form initially exuberant projections that are subsequently refined to achieve monosynaptic innervation of IHCs (45, 46). Here, we could trace the developmental progression of the SGN projections labeled by the expression of *Calb2-CreERT2* and *Lypd1-CreERT2* in the postnatal phase when the expression of these markers has been refined to subsets of SGNs with distinct innervation patterns onto IHCs. Both neuronal subtypes show by P7 preferences in their innervation specificity such that *Calb2-CreERT2* projections are rarely found on the modiolar side of IHCs, and *Lypd1-CreERT2* projections rarely on the pillar side of IHCs. However, the vast majority of labeled neurons in both mouse lines still form several branches that are consolidated to monosynaptic innervation by P28. It is remarkable that the time window for the refinement of nerve projections coincides with the time window when these neurons also refine their gene expression program to form mature type IA, IB, and IC neurons. Further studies are necessary to establish whether there is a causal link between molecular and synaptic refinement.

Previous studies in several species have demonstrated that type I SGNs have a wide range of SRs and that neurons with higher SRs have a lower threshold for activation compared to neurons with lower SRs (3, 31, 47–49). All studies have consistently identified a population of type I SGNs with very low SRs. Our findings now suggest that a subset of neurons in this population constitutes a distinct genetically defined cell population that can be captured by the expression of *Lypd1-CreERT2*. The properties of the remaining type I SGNs are more complex. In some species such as cats, SR distributions are bimodal, with a tail, that have been grouped as low, medium, and high SRs (7–12). In other species, a bimodal distribution is less obvious, and neurons seem to have a broad range of SRs along a continuum (19, 28–31). The pool of type I SGNs that are labeled by *Calb2-CreERT2* have a broader range of SRs indicative of more diverse features and suggest that a strict stratification of all SGNs into three molecular subclasses is not obvious, at least not with the *CreERT2* tools used here.

How this diversity is established within this pool of neurons is currently unclear. It has to be noted that besides intrinsic genetic differences in SGNs, diversity in other pre- and postsynaptic mechanisms including calcium channel activation, ribbon size and the specifics of the glutamate receptor field, and postsynaptic modulation by lateral efferent fibers also likely contribute to shaping the afferent physiological responses (15, 17, 20–27, 50–52). For example, a basic SR may be set by the number and properties of calcium channels presynaptically and could be further modulated postsynaptically. It is not clear, but a possibility, that the interaction between the hair cell presynapse and the SGN endings contributes to setting presynaptic properties; therefore, hypothetically, SGN diversity could also contribute to diverse presynaptic properties. Notably, olivocochlear efferent projections could play a role as they arrive in the IHC region shortly after birth (53) prior to the establishment of the SRs of cochlear afferents that occurs between P7 and P20 (54). In addition, efferent bundles have been observed close to the basal pole of IHCs (55), and the distance from the developing efferent innervation might be related to the size of AMPAR patches. Regardless of the mechanism, the variable response properties of SGNs are an important feature to allow for graded responses of these neurons to gradually increasing sound levels thus providing greater signaling capability (49, 56).

The availability of genetic tools as described here will allow one to test the functional contribution of molecularly and physiologically distinct SGN subgroups, for example, by analyzing response properties of neurons following their labeling with Cre-dependent genetically encoded fluorescence sensors that indicate neuronal activity in response to sound stimulation. In addition, it will be important to test the extent to which the expression of specific genes, for example, the expression levels of voltage-gated ion channels that are differentially expressed between type IA, IB, and IC SGNs (32–35) vary systematically with SRs. Since type I SGN subtypes show differential sensitivity to noise and aging (57), the genetic tools that we describe here will also be useful to further probe the mechanisms by which these neurons are affected in pathophysiological conditions and during aging.

Materials and Methods

Methods details are described in *SI Appendix*.

Mouse Lines. *Calb2-CreERT2* mice were obtained from JAX[B6(Cg) *Calb2tm2.1(cre/ERT2)Zjh/J*, Stock No: 013730]. These mice have a *CreERT2* knock-in allele at the *Calb2* locus. Lypd1-*CreERT2* mice were generated by CRISPR/Cas9 genomic editing to insert a 2TA cleavage peptide followed by *CreERT2* in front of the endogenous *Lypd1* stop codon. For experiments, only mice heterozygous for *CreERT2* were used.

Labeling of Nerve Fibers Using Ai9/Ai14 Reporter Mice and AAV Vectors. Tamoxifen induction in *Calb2-CreERT2;Ai9/Ai14* and *Lypd1-CreERT2;Ai9/Ai14* mice was performed by single intraperitoneal injection of tamoxifen (Sigma, T5648-1G) (0.1 mg per 1 g body weight). Alternatively, two doses of 4-hydroxytamoxifen (Sigma, H6278-50MG) (0.05 mg per 1 g body weight) were used. To achieve sparse labeling, animals were injected with lower doses of tamoxifen (50 µg/animal).

To produce very sparse labeling, we combined injection of Cre-dependent reporter viruses (pAAV.synP.DIO.EGFP.WPRE.hGH (AAV9–Addgene 100043 Lot: v25058, Titer: $4.3*10^{13}$ GC/mL) with tamoxifen induction as detailed in *SI Appendix*.

Immunofluorescence. For immunohistochemistry, cochleas were dissected from perfused mice, decalcified, stained with antibodies, and analyzed by fluorescence immunohistochemistry as described in *SI Appendix*.

Imaging and Image Analysis. Sections were imaged using a Zeiss 800 Confocal Laser Microscope. Images were processed using Imaris (version 9.6–9.7.1).

Loose-Patch Recordings in Acutely Excised Cochlear Coils. Loose-patch recordings from SGN bouton endings were performed to monitor SRs (19) as described in detail in *SI Appendix*. To achieve sparse labeling of SGN projections in *Calb2-CreERT2* and *Lypd1-CreERT2* mice, we injected them with low doses of tamoxifen (50 µg/animal) at P21 as described above. Recordings were performed at P28. Recordings were sampled between 20 and 50 kHz and low pass filtered at 10 kHz. Spike detection was performed in MiniAnalysis software (Synaptosoft; RRID:SCR_014441) and double-checked by eye. The SGN bouton endings chosen for recording were judged to be contacting the IHC on the pillar or the modiolar side before forming a loose-patch seal as described in *SI Appendix*.

The Shapiro–Wilk test was used to determine that SRs from electrophysiological recordings were not normally distributed. Therefore, the SRs between groups were compared using a Kruskal–Wallis test followed by a Dunn's multiple comparison. Results are reported as mean ± SD. Statistical tests are named in *Results* or Figure Legends with the statistical significance (*P*) and the number of cells (n). In the figures, the whiskers represent the minimum and maximum values, and *P* is defined as n.s. (not significant) $P > 0.05$; $*P < 0.05$; $**P < 0.01$; and $***P < 0.001$. Graphs of results were made in Prism 9 for MacOS and windows (version 9.1.2).

Data, Materials, and Software Availability. All study data are included in the article and/or *SI Appendix*. Mouse lines will be made available following processing of simple MTA forms.

ACKNOWLEDGMENTS. U.M. is a cofounder of Decibel Therapeutics and has stocks and stock options. This work was supported by support from the NIH (RO1DC005965 and RO1DC019514 to U.M.; R01DC006476 to E.G.; 5T32DC000023-37) and the Rubenstein Fund for Hearing Research. U.M. is a Bloomberg Distinguished Professor for Neuroscience and Biology, and Elisabeth Glowatzki is the George T. Nager M.D. Professor for Otolaryngology Head and Neck Surgery.

Author affiliations: [a]The Solomon H. Snyder Department of Neuroscience, Johns Hopkins University School of Medicine, Baltimore, MD 21205; [b]Department of Otolaryngology-Head and Neck Surgery, Johns Hopkins University School of Medicine, Baltimore, MD 21205; [c]National Institute of Biological Science, Beijing 102206, China; and [d]Tsinghua Institute of Multidisciplinary Biomedical Research, Tsinghua University, Beijing 100084, China

Author contributions: C.S., P.F.Y.V., R.T.B., S.S., D.O.J.R., M.M., E.G., and U.M. designed research; C.S., P.F.Y.V., R.T.B., S.S., D.O.J.R., and M.M. performed research; C.S., R.T.B., and S.S. contributed new reagents/analytic tools; C.S., P.F.Y.V., R.T.B., S.S., D.O.J.R., M.M., E.G., and U.M. analyzed data; and C.S., E.G., and U.M. wrote the paper.

1. J. R. Sanes, R. H. Masland, The types of retinal ganglion cells: Current status and implications for neuronal classification. *Annu. Rev. Neurosci.* **38**, 221–246 (2015).
2. T. A. Seabrook, T. J. Burbridge, M. C. Crair, A. D. Huberman, Architecture, function, and assembly of the mouse visual system. *Annu. Rev. Neurosci.* **40**, 499–538 (2017).
3. P. Heil, A. J. Peterson, Basic response properties of auditory nerve fibers: A review. *Cell Tissue Res.* **361**, 129–158 (2015).
4. A. J. Oxenham, C. J. Plack, A behavioral measure of basilar-membrane nonlinearity in listeners with normal and impaired hearing. *J. Acoust. Soc. Am.* **101**, 3666–3675 (1997).
5. D. O. J. Reijntjes, S. J. Pyott, The afferent signaling complex: Regulation of type I spiral ganglion neuron responses in the auditory periphery. *Hear Res.* **336**, 1–16 (2016).
6. R. L. Davis, Q. Liu, Complex primary afferents: What the distribution of electrophysiologically-relevant phenotypes within the spiral ganglion tells us about peripheral neural coding. *Hear Res.* **276**, 34–43 (2011).
7. E. Borg, B. Engstrom, G. Linde, K. Marklund, Eighth nerve fiber firing features in normal-hearing rabbits. *Hear Res.* **36**, 191–201 (1988).
8. A. C. Furman, S. G. Kujawa, M. C. Liberman, Noise-induced cochlear neuropathy is selective for fibers with low spontaneous rates. *J. Neurophysiol.* **110**, 577–586 (2013).
9. M. C. Liberman, Auditory-nerve response from cats raised in a low-noise chamber. *J. Acoust. Soc. Am.* **63**, 442–455 (1978).
10. E. M. Relkin, J. R. Doucet, Recovery from prior stimulation. I: Relationship to spontaneous firing rates of primary auditory neurons. *Hear Res.* **55**, 215–222 (1991).
11. C. J. Sumner, A. R. Palmer, Auditory nerve fibre responses in the ferret. *Eur. J. Neurosci.* **36**, 2428–2439 (2012).
12. A. N. Temchin, N. C. Rich, M. A. Ruggero, Threshold tuning curves of chinchilla auditory nerve fibers. II. Dependence on spontaneous activity and relation to cochlear nonlinearity. *J. Neurophysiol.* **100**, 2899–2906 (2008).
13. M. C. Liberman, Single-neuron labeling in the cat auditory nerve. *Science* **216**, 1239–1241 (1982).
14. M. C. Liberman, L. W. Dodds, S. Pierce, Afferent and efferent innervation of the cat cochlea: Quantitative analysis with light and electron microscopy. *J. Comp. Neurol.* **301**, 443–460 (1990).
15. A. Merchan-Perez, M. C. Liberman, Ultrastructural differences among afferent synapses on cochlear hair cells: Correlations with spontaneous discharge rate. *J. Comp. Neurol.* **371**, 208–221 (1996).
16. J. Tsuji, M. C. Liberman, Intracellular labeling of auditory nerve fibers in guinea pig: Central and peripheral projections. *J. Comp. Neurol.* **381**, 188–202 (1997).
17. L. D. Liberman, H. Wang, M. C. Liberman, Opposing gradients of ribbon size and AMPA receptor expression underlie sensitivity differences among cochlear-nerve/hair-cell synapses. *J. Neurosci.* **31**, 801–808 (2011).
18. A. L. Markowitz, R. Kalluri, Gradients in the biophysical properties of neonatal auditory neurons align with synaptic contact position and the intensity coding map of inner hair cells. *Elife* **9**, e55378 (2020).
19. J. S. Wu, E. D. Young, E. Glowatzki, Maturation of spontaneous firing properties after hearing onset in rat auditory nerve fibers: Spontaneous rates, refractoriness, and interfiber correlations. *J. Neurosci.* **36**, 10584–10597 (2016).
20. T. Frank, D. Khimich, A. Neef, T. Moser, Mechanisms contributing to synaptic Ca2+ signals and their heterogeneity in hair cells *Proc. Natl. Acad. Sci. U.S.A.* **106**, 4483–4488 (2009).
21. L. D. Liberman, M. C. Liberman, Postnatal maturation of auditory-nerve heterogeneity, as seen in spatial gradients of synapse morphology in the inner hair cell area. *Hear Res.* **339**, 12–22 (2016).
22. A. C. Meyer *et al.*, Tuning of synapse number, structure and function in the cochlea. *Nat. Neurosci.* **12**, 444–453 (2009).
23. M. Niwa, E. D. Young, E. Glowatzki, A. J. Ricci, Functional subgroups of cochlear inner hair cell ribbon synapses differently modulate their EPSC properties in response to stimulation. *J. Neurophysiol.* **125**, 2461–2479 (2021).
24. T. L. Ohn *et al.*, Hair cells use active zones with different voltage dependence of Ca2+ influx to decompose sounds into complementary neural codes. *Proc. Natl. Acad. Sci. U.S.A.* **113**, E4716–4725 (2016).
25. O. D. Ozcete, T. Moser, A sensory cell diversifies its output by varying Ca(2+) influx-release coupling among active zones *EMBO J.* **40**, e106010 (2021).
26. S. A. Payne *et al.*, Maturation of heterogeneity in afferent synapse ultrastructure in the Mouse Cochlea. *Front. Synaptic. Neurosci.* **13**, 678575 (2021).
27. D. O. J. Reijntjes, C. Koppl, S. J. Pyott, Volume gradients in inner hair cell-auditory nerve fiber pre- and postsynaptic proteins differ across mouse strains. *Hear Res.* **390**, 107933 (2020).
28. A. el Barbary, Auditory nerve of the normal and jaundiced rat. I. Spontaneous discharge rate and cochlear nerve histology. *Hear Res.* **54**, 75–90 (1991).
29. K. K. Ohlemiller, S. M. Echteler, Functional correlates of characteristic frequency in single cochlear nerve fibers of the Mongolian gerbil. *J. Comp. Physiol. A* **167**, 329–338 (1990).
30. R. A. Schmiedt, Spontaneous rates, thresholds and tuning of auditory-nerve fibers in the gerbil: Comparisons to cat data. *Hear Res.* **42**, 23–35 (1989).
31. A. M. Taberner, M. C. Liberman, Response properties of single auditory nerve fibers in the mouse. *J. Neurophysiol.* **93**, 557–569 (2005).
32. C. Petitpre *et al.*, Neuronal heterogeneity and stereotyped connectivity in the auditory afferent system. *Nat. Commun.* **9**, 3691 (2018).
33. B. R. Shrestha *et al.*, Sensory neuron diversity in the inner ear is shaped by activity. *Cell* **174**, 1229–1246.e1217 (2018).
34. S. Sun *et al.*, Hair cell mechanotransduction regulates spontaneous activity and sprial ganglion subtype specification in the auditory system. *Cell* **174**, 1247–1263.e15 (2018).
35. C. Petitpre *et al.*, Single-cell RNA-sequencing analysis of the developing mouse inner ear identifies molecular logic of auditory neuron diversification. *Nat. Commun.* **13**, 3878 (2022).
36. H. Taniguchi *et al.*, A resource of Cre driver lines for genetic targeting of GABAergic neurons in cerebral cortex. *Neuron* **71**, 995–1013 (2011).
37. M. L. L. Donnelly *et al.*, Analysis of the aphthovirus 2A/2B polyprotein "cleavage" mechanism indicates not a proteolytic reaction, but a novel translational effect: A putative ribosomal "skip". *J. Gen. Virol.* **82**, 1013–1025 (2001).
38. L. Madisen *et al.*, A robust and high-throughput Cre reporting and characterization system for the whole mouse brain. *Nat. Neurosci.* **13**, 133–140 (2010).
39. M. Barclay, A. F. Ryan, G. D. Housley, Type I vs type II spiral ganglion neurons exhibit differential survival and neuritogenesis during cochlear development. *Neural. Dev.* **6**, 33 (2011).
40. F. Lallemend *et al.*, New insights into peripherin expression in cochlear neurons. *Neuroscience* **150**, 212–222 (2007).
41. S. Sun, C. Siebald, U. Muller, Subtype maturation of spiral ganglion neurons. *Curr. Opin. Otolaryngol. Head Neck Surg.* **29**, 391–399 (2021).
42. C. J. Dechesne, D. Rabejac, G. Desmadryl, Development of calretinin immunoreactivity in the mouse inner ear. *J. Comp. Neurol.* **346**, 517–529 (1994).
43. T. R. Sanders, M. W. Kelley, Specification of neuronal subtypes in the spiral ganglion begins prior to birth in the mouse. *Proc. Natl. Acad. Sci. U.S.A.* **119**, e2203935119 (2022).
44. R. Fettiplace, Hair cell transduction, tuning, and synaptic transmission in the Mammalian Cochlea. *Compr. Physiol.* **7**, 1197–1227 (2017).
45. J. M. Appler, L. V. Goodrich, Connecting the ear to the brain: Molecular mechanisms of auditory circuit assembly. *Prog. Neurobiol.* **93**, 488–508 (2011).
46. T. M. Coate, M. W. Kelley, Making connections in the inner ear: Recent insights into the development of spiral ganglion neurons and their connectivity with sensory hair cells. *Semin. Cell Dev. Biol.* **24**, 460–469 (2013).
47. N. Y. Kiang, T. Watanabe, E. C. Thomas, L. F. Clark, *Discharge Patterns of Single Fibers in the Cat's Auditory Nerve* (Spontaneous Activty Massachusetts Institute of Technology, 1965).
48. M. B. Sachs, P. J. Abbas, Rate versus level functions for auditory-nerve fibers in cats: Tone-burst stimuli. *J. Acoust. Soc. Am.* **56**, 1835–1847 (1974).
49. M. B. Sachs, R. L. Winslow, B. H. Sokolowski, A computational model for rate-level functions from cat auditory-nerve fibers. *Hear Res.* **41**, 61–69 (1989).
50. D. Felix, K. Ehrenberger, The efferent modulation of mammalian inner hair cell afferents. *Hear Res.* **64**, 1–5 (1992).
51. J. Neef *et al.*, Quantitative optical nanophysiology of Ca(2+) signaling at inner hair cell active zones. *Nat. Commun.* **9**, 290 (2018).
52. J. Ruel *et al.*, Dopamine inhibition of auditory nerve activity in the adult mammalian cochlea. *Eur. J. Neurosci.* **14**, 977–986 (2001).
53. R. Pujol, E. Carlier, C. Devigne, Different patterns of cochlear innervation during the development of the kitten. *J. Comp. Neurol.* **177**, 529–536 (1978).
54. E. J. Walsh, J. McGee, Postnatal development of auditory nerve and cochlear nucleus neuronal responses in kittens. *Hear Res.* **28**, 97–116 (1987).
55. M. C. Liberman, Efferent synapses in the inner hair cell area of the cat cochlea: An electron microscopic study of serial sections. *Hear Res.* **3**, 189–204 (1980).
56. G. K. Yates, I. M. Winter, D. Robertson, Basilar membrane nonlinearity determines auditory nerve rate-intensity functions and cochlear dynamic range. *Hear Res.* **45**, 203–219 (1990).
57. M. C. Liberman, Noise-induced and age-related hearing loss: New perspectives and potential therapies. *F1000Res* **6**, 927 (2017).